# Failure mechanisms of graphene under tension

Chris A. Marianetti[1*] and Hannah G. Yevick[2]

[1]Department of Applied Physics and Applied Mathematics, Columbia University
[2]Department of Physics, Columbia University
500 West 120th St., 1144 Mudd Hall, New York, NY 10027, USA

[*]E-mail: chris.marianetti@columbia.edu.

**Recent experiments established pure graphene as the strongest material known to mankind, further invigorating the question of how graphene fails. Using density functional theory, we reveal the mechanisms of mechanical failure of pure graphene under a generic state of tension. One failure mechanism is a novel soft-mode phonon instability of the $K_1$-mode, whereby the graphene sheet undergoes a phase transition and is driven towards isolated benzene rings resulting in a reduction of strength. The other is the usual elastic instability corresponding to a maximum in the stress-strain curve. Our results indicate that finite wave vector soft modes can be the key factor in limiting the strength of monolayer materials.**

The mechanical failure of materials is usually a complex process which may involve defects at a variety of length scales, such as dislocations, grain boundaries, cracks, etc. The complexity and statistical nature of these defects cause mechanical failure to be extremely dependent on not only the type of material, but also on the manner in which the material was synthesized. To the contrary, ideal strength, which can be defined as the maximum attainable stress under a

uniform strain field in the absence of any instabilities, is an intrinsic property of a material (*1*). Perhaps the simplest instability is the so-called elastic instability, whereby a maximum in the stress-strain relation is achieved while retaining the symmetry of strained lattice. There has been a significant experimental effort throughout the past century to prepare sufficiently pure samples such that the ideal strength could be probed, including early experiments with fine glass rods and steel wires (*2*). Recently, the measurement of ideal strength has been achieved in the case of graphene (*3*), a monolayer of carbon. Using nanoindentation, Lee et al managed to strain graphene until failure under conditions which appear to be very nearly ideal (*4*). This experiment reinvigorates the fundamental question of how and why a material fails under ideal conditions. The answer lies within the forces which bond a material together. Computing these forces from the first-principles of quantum mechanics is made possible by intelligent approximations to the quantum many-body problem, such as the local density approximation (LDA) of density functional theory (DFT) (*5, 6*), in addition to plentiful computational resources. While LDA may qualitatively break down in certain situations where the electronic correlations are strong (*7*), it works extremely well in materials with relatively large electronic bands such as graphene. Therefore, one can reliably explore the mechanical properties of graphene from first-principles. In this study, we use DFT to determine the mechanism of mechanical failure for an arbitrary state of tension.

To determine the elastic instability of a material, DFT can be used to generate the forces as a function of strain, and such studies were performed once sufficient computational power was available (see reference (*8*) and references therein). However, there is no guarantee that the structure will remain stable with respect to *inhomogeneous* deformations under strain. Indeed, a structure may become unstable and transform to a different structure with a lower ideal strength. In order to determine if a structure is mechanically stable, one needs to consider lattice vibrations and confirm that all of the phonon energies are real and positive (*9*). If any of the

phonon energies were to go to zero, there would be no energy barrier for the crystal to distort along the zero-energy phonon mode. Therefore, the phonon spectrum is the fundamental entity which dictates structural stability. Phonon modes with zero or very small energies, excluding the acoustic phonons for $k \rightarrow 0$, are usually termed "soft-modes" (*10*). There are numerous structural phase transitions in which the two phases are directly connected by a soft-mode, and the concept of the soft-mode gained prominence in the context of elucidating the ferroelectric transition in $BaTiO_3$ (*11, 12*). In this work, we demonstrate that a soft-mode is responsible for a phase transition and the resulting mechanical failure of graphene in certain states of tension. Previous DFT studies of *bulk* systems such as Ni (*13*) and Si (*14*) have demonstrated that non-trivial acoustic phonon instabilities may precede the usual elastic instability for certain states of strain and therefore limit the ideal strength of the material. However, these scenarios are extremely difficult to decipher experimentally, even indirectly, due to defects and plastic deformation, while our predictions in graphene may be directly tested experimentally.

In the case of graphene, previous phonon calculations have determined that the elastic instability is the mechanism of failure for uniaxial strain in the armchair or zig-zag directions (*15*) (ie. $x$ and $y$ directions in panel C/D/E of Figure 2, respectively). However, the mode of failure in a more general state of strain has never been considered. In this work, we computed the phonons using the displacement method (*16*), where the forces are generated using DFT. All DFT calculations were performed using the Vienna ab-initio simulation program (VASP) (*17–20*), which uses a plane-wave basis and projector-augmented wave (PAW) potentials (*21*). An energy cutoff of $375eV$ was used with the soft VASP carbon PAW, and k-point meshes of $27 \times 27$, with respect to the primitive cell. A state of strain was constructed by applying the strain and allowing all cell internal coordinates to relax. Supercells of $9 \times 9$ times the primitive cell were used when computing the force constants. The displacement method involves computing the real space force constants between atoms by displacing an atom and evaluating the resulting

forces. Previous work has established that the displacement method is accurate for unstrained graphene (*22*). In Figure 1 we present the phonons for equibiaxial strains ranging from zero to $\epsilon_A = (\epsilon_x + \epsilon_y)/\sqrt{2} = 0.212$, where $\epsilon_i$ is the nominal strain $\ell_i/\ell_{io} - 1$. In Figure 1A, we reproduce the phonons for unstrained graphene, showing excellent agreement with previous work (*15*,*22*). Due to symmetry, all phonon modes contain purely either out-of-plane or in-plane atomic displacements. Three acoustic branches and three optical branches are present, and the $z$-axis acoustic branch has a nonlinear dispersion at small wave vector as expected for a monolayer. In Figure 1B, the phonons are shown for the case of an equibiaxial strain of $\epsilon_A = 0.106$. A significant softening of the in-plane phonons is observed, which is to be expected given that all the in-plane distances are increasing uniformly. The out-of-plane phonons change less in general, and one notable change is that the quadratic dispersion of the acoustic out-of-plane mode becomes closer to linearity. In Figure 1C, corresponding to a strain of $\epsilon_A = 0.205$, it becomes clear that certain phonon modes are softening at a much higher rate than others. In particular, the $K_1$ mode at the $K$-point is rapidly dropping towards zero. Upon reaching a strain of $\epsilon_A = 0.212$ (see Figure 1D), the $K_1$-mode has become imaginary resulting in a soft-mode. This implies that the structure has become unstable and will undergo a phase transition by distorting along the $K_1$-mode. Group theory alone dictates the nature of this $K_1$-mode, and by considering linear combinations of both $K$ and $K'$ one arrives at two distinct real distortions (*23*) (see figure 2C/D/E). These modes can be classified as the $A_1$ and $B_1$ irreducible representations of the $C_{6v}$ point group. The positive amplitude of the $A_1$ mode can be viewed as the formation of individual benzene rings where all edge-sharing benzene neighbors have been annihilated, while both the $B_1$ and negative $A_1$ amplitudes form dimerized structures. While the $A_1$ and $B_1$ modes transform differently under $C_{6v}$, these modes form a 2-fold representation when including the lattice translations. Below we show the positive $A_1$ mode is most energetically favorable when including anharmonicity.

Given that the $K_1$-mode has a reasonably short wavelength, one can directly explore the properties of this mode with a 6-atom unit cell, which is three times the size of the primitive cell (see Figure 2C/D/E). We shall refer to this enlarged unit cell as the $K$-cell hereafter. The energy is computed as a function of the amplitude of the $A_1$-mode and $B_1$-mode at a series of different equibiaxial strains (see Figure 2A/B). The curvature at zero amplitude (ie. $k/2$) gives the phonon energy $\hbar\sqrt{k/m}$, which must be identical for these degenerate modes. As the strain is increased, the modes continually becomes softer and eventually the curvature at zero amplitude goes to zero and the modes becomes soft simultaneously. This analysis predicts the soft mode to occur at $\epsilon_A = 0.213$, independently confirming the results of our phonons which yield a soft mode at $\epsilon_A = 0.205 - 0.212$. Further strain results in a double-well potential, where the well depth and amplitude increases with increasing strain. In the absence of anharmonicity, one would find the well known "Mexican hat" potential characteristic of a two-fold representation, but anharmonicity results in the more usual "warped Mexican hat" potential (see Figure 2A inset). As shown in Figure 2, the minimum energy corresponds to the positive amplitude of the pure positive $A_1$ mode (or identically $-\frac{1}{2}A_1 \pm \frac{\sqrt{3}}{2}B_1$ ). This is physically reasonable given that the positive $A_1$ mode forms benzene rings while the other distortions result in dimerized structures.

It should be emphasized that at this point one does not know if the material will fracture, only that a phase transition will occur. Therefore, we must explore the strength and stability of this new phase of strained graphene. The stress as a function of the equibiaxial strain is computed for both the primitive unit cell and the $K$-cell (see Figure 3). For the primitive cell, the curve is smooth and the elastic instability occurs at a strain of $\epsilon_A = (\epsilon_x + \epsilon_y)/\sqrt{2} = 0.307$. However, the primitive unit cell does not have the freedom to distort along the $K_1$-mode as the primitive translational symmetry is enforced in the calculation (ie. the primitive cell is smaller than the wavelength of the $K_1$-mode). The same curve can now be analyzed for the $K$-cell. The phonon-

instability is clearly illustrated by a discontinuity in the curve at $\epsilon_A = 0.213$ (see inset of Figure 3), in excellent agreement with our preceding two calculations. Upon activation of the $K_1$-mode, the force rapidly drops, and is subsequently nearly flat until decreasing. Therefore, this new phase which forms is essentially mechanically unstable, and there is no need to recompute the phonons for this new phase. As a result, the soft $K_1$-mode can be seen not only as the precursor to a phase transition as in soft-mode theory, but also as a soft-mode which leads directly to mechanical failure.

The above analysis has revealed that for equibiaxial strain the mode of failure of graphene is radically different than the usual elastic instability which is observed for uniaxial strain in the zig-zag or armchair directions. Therefore, the question arises as to when the elastic instability is the failure mode versus the $K_1$-mode instability for a generic state of tension. In order to resolve this we have computed the stress versus strain for both the primitive unit cell and the $K$-cell, as above, for all possible linear combinations of tensile strain in the zig-zag and armchair directions (see Figure 4A). This two-dimensional space of strains can be characterized in polar coordinates with an angle and a radius, and $\theta = 45$ corresponds to equibiaxial strain. As shown in Figure 4, the plot is naturally separated into three regions. In the first and third region the elastic instability precedes the $K_1$-mode instability, and therefore the failure mechanism is the elastic instability. On the contrary, in the second region the $K_1$-mode instability occurs first and therefore limits the strength of the material. Therefore, strains near uniaxiality fail via the elastic instability while strains near equibiaxiality fail via the $K_1$-mode instability. It is worth noting the degree of symmetry in this plot. The $K_1$-mode instability is nearly invariant for a mirror line placed at $\theta = 45$, despite the fact that there is no such lattice symmetry. Alternatively, the elastic curve has some observable differences. The stress in the $x$ and $y$ directions at failure (ie. along the $K$-cell line in Figure 4A) is plotted as a function of $\theta$ (see Figure 4B), indicating the stress necessary to realize the state of strain at failure.

This analysis is not yet exhaustive due to the fact that graphene is anisotropic, and therefore shear strain would have to be included in the present coordinate system to enumerate every possible state of tension. Alternatively, one could repeat the above analysis for every possible rotation of the coordinate system which is not generated by a member of the point group of graphene. This corresponds to generating Figure 4A for every possible rotation of the coordinate system between zero and 15 degrees. We have rotated the coordinate system in three degree increments and regenerated Figure 4 at each increment (see Figure 4C for $15$ degree rotation). Clearly, $\theta = 45$, which corresponds to equibiaxial strain, will be invariant to any rotation. Conveniently, all of the results for the different rotations are bounded by the envelope curves created by superimposing Figure 4A and 4C. All rotation curves progress monotonically with rotation between the limits of the envelope. The envelope for the $K_1$-mode instability is extremely narrow, reflecting the insensitivity to rotation (ie. shear). It should be noted that Figure 4C is symmetric about $\theta = 45$ due to a mirror line which maps $x' \leftrightarrow y'$.

Our prediction of the soft $K_1$-mode may be directly verified experimentally by measuring the phonon dispersion as a function of strain. Neutrons have commonly been used to measure phonon dispersion as a function of temperature, allowing the detection of soft modes as precursors to phase transitions in a variety of different *bulk* systems (*24*). In the case of a *monolayer*, measuring the phonon spectrum is a much more difficult venture as not enough material is present to use neutrons. Electrons have been used to measure the surface phonons of graphite, which is an excellent approximation to graphene, both using reflection electron-energy-loss spectroscopy (*25*) and high-resolution electron-energy-loss spectroscopy (*26*). Therefore, the phonons could potentially be measured directly for graphene. The challenge in this particular case would be the fact that the graphene would have to be strained in-situ. Another more indirect probe would be Raman spectroscopy (*23*), which has already been performed for graphene under uniaxial tension (*27*).

It is instructive to make a comparison of our results with existing experimental observations. The experiments of Lee et al suspended graphene over cylindrical holes in a $SiO_2$ substrate and used an atomic force microscope to impinge upon the graphene until failure occurred (*4*). They assumed that the strain in the sample beneath the indenter tip may be approximated as equibiaxial. The stress was fit to second order in the equibiaxial strain and resulted in a Lagrangian breaking strain of $\epsilon_x = \epsilon_y = 0.250$, which corresponds to a nominal strain of $\epsilon_x = \epsilon_y = 0.225$. Unexpectedly, this far exceeds the breaking strain as dictated by the $K_1$-mode of $\epsilon_x = \epsilon_y = 0.151$. Therefore, it is clear that theory and experiment are not operating under identical conditions, and it is necessary to detail all significant differences. Firstly, our calculations are performed at zero-temperature, while the experiments are performed at room temperature. Secondly, the experiment could be influenced by the presence of the nano-indenter tip or other elements which may react with the graphene layer. Finally, the experiment is assumed to be in a state of equibiaxial strain while our calculations are by construction. Any and all of these differences may be linked to the difference between theory and experiment. Interestingly, the results of Lee et al are in reasonable agreement with our results for the elastic instability of equibiaxial strain (ie. $\epsilon_x = \epsilon_y = 0.216$). This is suggestive that perhaps somehow the $K_1$-mode is being stabilized in the nanoindentation experiment. One possibility is that the $K_1$-mode is being stabilized by temperature, as the experiments are performed at room temperature. Given the well depth of $175meV$ of the $K_1$-mode for a strain of $\epsilon_x = \epsilon_y = 0.22$ (see Figure 2), it appears unlikely that temperature alone will account for this difference. However, temperature will clearly influence when the $K_1$-mode activates. This issue can be resolved by bridging theory and experiment in future work. Nanoindentation experiments may be performed at low temperatures, and molecular dynamics simulations may be performed at high temperature and in a geometry similar to experiment.

In conclusion, we have determined the failure mechanisms of graphene under ideal condi-

tions using DFT calculations. Graphene fails via the usual elastic instability for any uniaxial strain. In the case of equibiaxial strain, graphene exhibits a novel soft-mode phonon instability at the $K$-point which results in a phase transition into an unstable phase and leads to mechanical failure. This $K_1$-mode instability corresponds to the graphene sheet distorting towards isolated benzene rings, and it goes soft for $\epsilon_A = (\epsilon_x + \epsilon_y)/\sqrt{2} = 0.213$ which significantly precedes the elastic instability at $\epsilon_A = 0.307$. We have mapped out the elastic failure and $K_1$-mode failure for all possible tensile strain states, documenting the transition between the two modes. Further experiments have been suggested to directly test our prediction of the softening of the $K_1$-mode.

We gratefully acknowledge support from NSF via Grant No. CMMI-0927891. We thank J.W. Kysar, M.E. Manley, and J. Hone for fruitful conversations.

# References and Notes

1. T. Zhu, J. Li, S. Ogata, S. Yip, *MRS Bulletin* **34**, 167 (2009).

2. E. Orowan, *Rep. Prog. Phys.* **12**, 185 (1949).

3. A. K. Geim, K. S. Novoselov, *Nature Materials* **6**, 183 (2007).

4. C. Lee, X. D. Wei, J. W. Kysar, J. Hone, *Science* **321**, 385 (2008).

5. P. Hohenberg, W. Kohn, *Phys. Rev. B* **136**, B864 (1964).

6. W. Kohn, L. J. Sham, *Physical Review* **140**, 1133 (1965).

7. G. Kotliar, *et al.*, *Rev. Mod. Phys.* **78**, 865 (2006).

8. J. W. Morris, C. R. Krenn, *Phil. Mag. A* **80**, 2827 (2000).

9. M. T. Dove, *Introduction to Lattice Dynamics* (Cambridge University Press, New York, 2005).

10. J. D. Axe, G. Shirane, *Physics Today* **26**, 32 (1973).

11. W. Cochran, *Advances In Physics* **9**, 387 (1960).

12. V. L. Ginzburg, *Physics-uspekhi* **44**, 1037 (2001).

13. D. M. Clatterbuck, C. R. Krenn, M. L. Cohen, J. W. Morris, *Phys. Rev. Lett.* **91**, 135501 (2003).

14. S. M. M. Dubois, G. M. Rignanese, T. Pardoen, J. C. Charlier, *Phys. Rev. B* **74**, 235203 (2006).

15. F. Liu, P. M. Ming, J. Li, *Phys. Rev. B* **76**, 064120 (2007).

16. A. VandeWalle, G. Ceder, *Rev. Mod. Phys.* **74**, 11 (2002).

17. G. Kresse, J. Hafner, *Phys. Rev. B* **47**, 558 (1993).

18. G. Kresse, J. Hafner, *Phys. Rev. B* **49**, 14251 (1994).

19. G. Kresse, J. Furthmuller, *Computational Materials Science* **6**, 15 (1996).

20. G. Kresse, J. Furthmuller, *Phys. Rev. B* **54**, 11169 (1996).

21. G. Kresse, D. Joubert, *Phys. Rev. B* **59**, 1758 (1999).

22. O. Dubay, G. Kresse, *Phys. Rev. B* **69**, 089906 (2004).

23. D. M. Basko, I. L. Aleiner, *Phys. Rev. B* **77**, 041409 (2008).

24. G. Shirane, *Rev. Mod. Phys.* **46**, 437 (1974).

25. C. Oshima, T. Aizawa, R. Souda, Y. Ishizawa, Y. Sumiyoshi, *Solid State Communications* **65**, 1601 (1988).

26. S. Siebentritt, R. Pues, K. H. Rieder, A. M. Shikin, *Surface Review And Letters* **5**, 427 (1998).

27. M. Y. Huang, *et al.*, *Proc. Natl. Acad. Sci.* **106**, 7304 (2009).

**Fig. 1.**(**A-E**) The phonons of graphene for different levels of equibiaxial strain. Blue lines indicate the phonons within the plane while red lines indicate phonons out of the plane. The $k$-point labels $\Gamma, M, K$ correspond to
$(0,0),(0.5,0),(1/3.,1/3.)$, respectively, in fractions of the reciprocal lattice vectors. A primitive cell of $\vec{a}_1 = (a\sqrt{3}/2, -a/2), \vec{a}_2 = (0, a)$ was used, where $a$ is the nearest-neighbor bond length. The different panels correspond to various levels of equibiaxial (ie. $\epsilon_x = \epsilon_y$) strain $\epsilon_A = (\epsilon_x + \epsilon_y)/\sqrt{2}$. A black arrow is used to identify the $K_1$ mode. A soft-mode can clearly be identified at the $K$-point for $\epsilon_A = 0.212$.

**Fig. 2.** (**A**) The energy as a function of the $A_1$ phonon amplitude for equibiaxial strain $\epsilon_A = (\epsilon_x+\epsilon_y)/\sqrt{2} = 0-0.311$ in increments of $\sqrt{2}/100$. The line color changes from green to yellow to red as strain increases. The phonon goes soft between the 15th and 16th curve corresponding to a strain of $\epsilon_A = 0.212 - 0.226$. The inset of panel A is a contour plot of the energy vs the $A_1$ and $B_1$ phonon amplitudes for a strain of $\epsilon_A = 0.311$. (**B**) The repeat of panel A for the $B_1$ phonon. (**C,D,E**) The negative $A_1$, positive $A_1$, and $B_1$ phonons, respectively ($B_1$ mode is symmetric). The undistorted lattice is shown in grey. The unit cell of the distorted structure (ie. the $K$-cell) is denoted with dotted purple lines. For illustrative purposes, the amplitudes shown corresponds to 2.5 times the amplitude for the respective well minima and $\epsilon_A = 0.311$.

**Fig. 3.** Nominal stress vs. equibiaxial strain for a primitive unit cell (blue line) and the $K$-cell (red line). The inset shows a magnified view of where the $K_1$-mode goes soft, as indicated by a discontinuity in the curve.

**Fig. 4.** (**A**) The maximum stable strain for the primitive unit cell (blue curve) and the $K$-cell (red curve) as a function of all possible linear combinations of zig-zag and armchair uniaxial tensile strains. A given direction of strain corresponds to an angle $\theta = 0 - 90$. Failure occurs via the $K_1$-mode in region II and via the elastic instability in region I and III. (**B**) The nominal stress in the $x$ and $y$ directions for all points along the $K$-cell curve in panel A. (**C**) The same

as panel A, except uniaxial strains are applied in the $x'$ and $y'$ directions, which correspond to a $15$ degree rotation of the coordinate system.

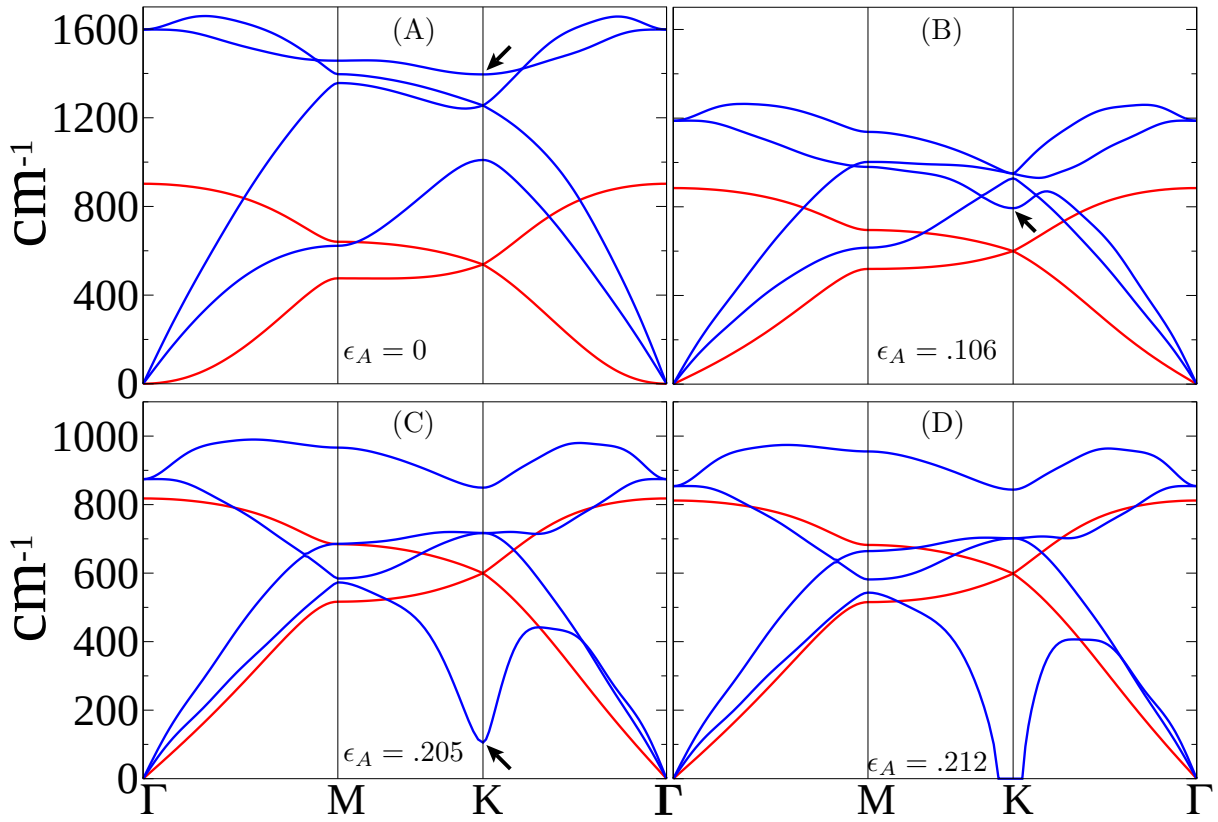


Figure 1:

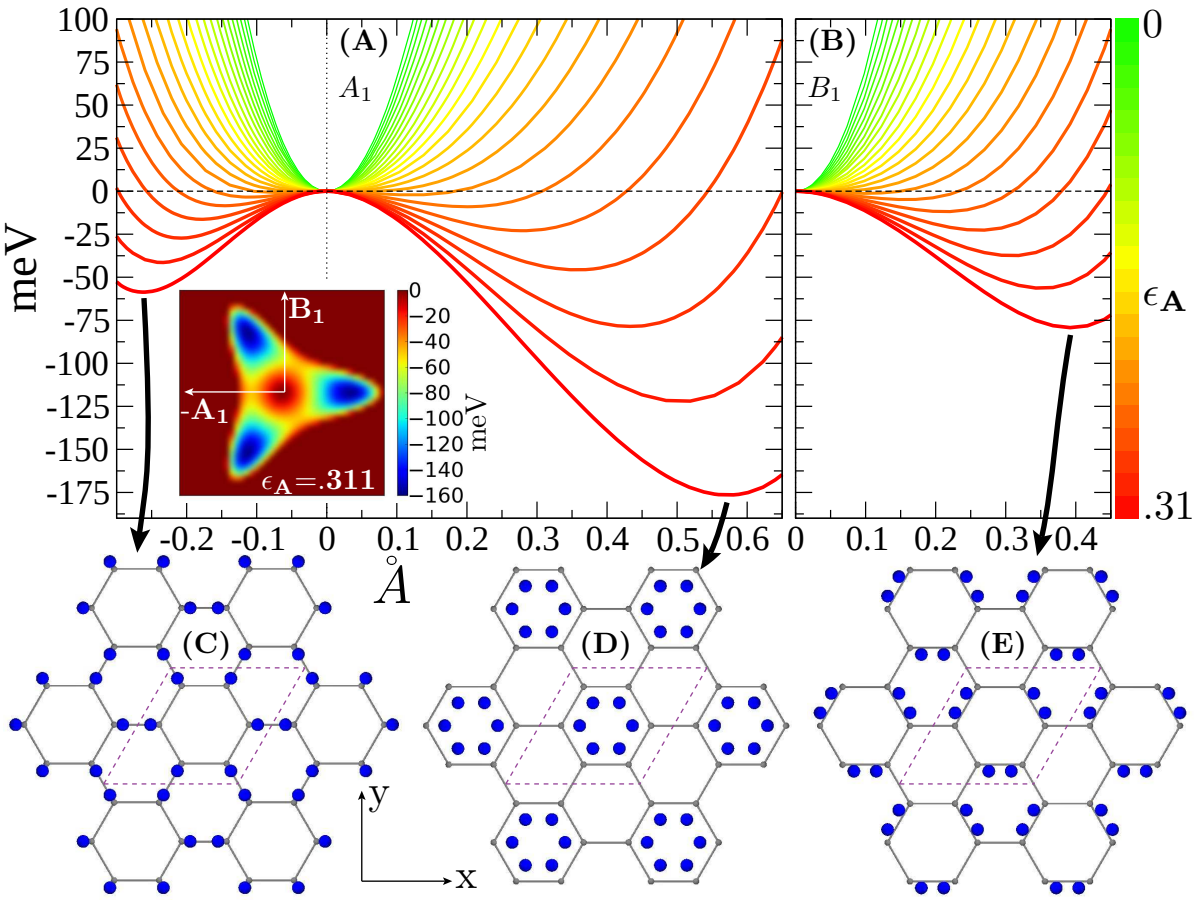
(A)
$A_1$
(B)
$B_1$
meV
100
75
50
25
0
-25
-50
-75
-100
-125
-150
-175
-0.2 -0.1 0 0.1 0.2 0.3 0.4 0.5 0.6
0 0.1 0.2 0.3 0.4
Å
$\epsilon_A$
0
.31
$B_1$
$-A_1$
$\epsilon_A$=.311
0
-20
-40
-60
-80
-100
-120
-140
-160
meV
(C)
(D)
(E)
y
x

Figure 2:

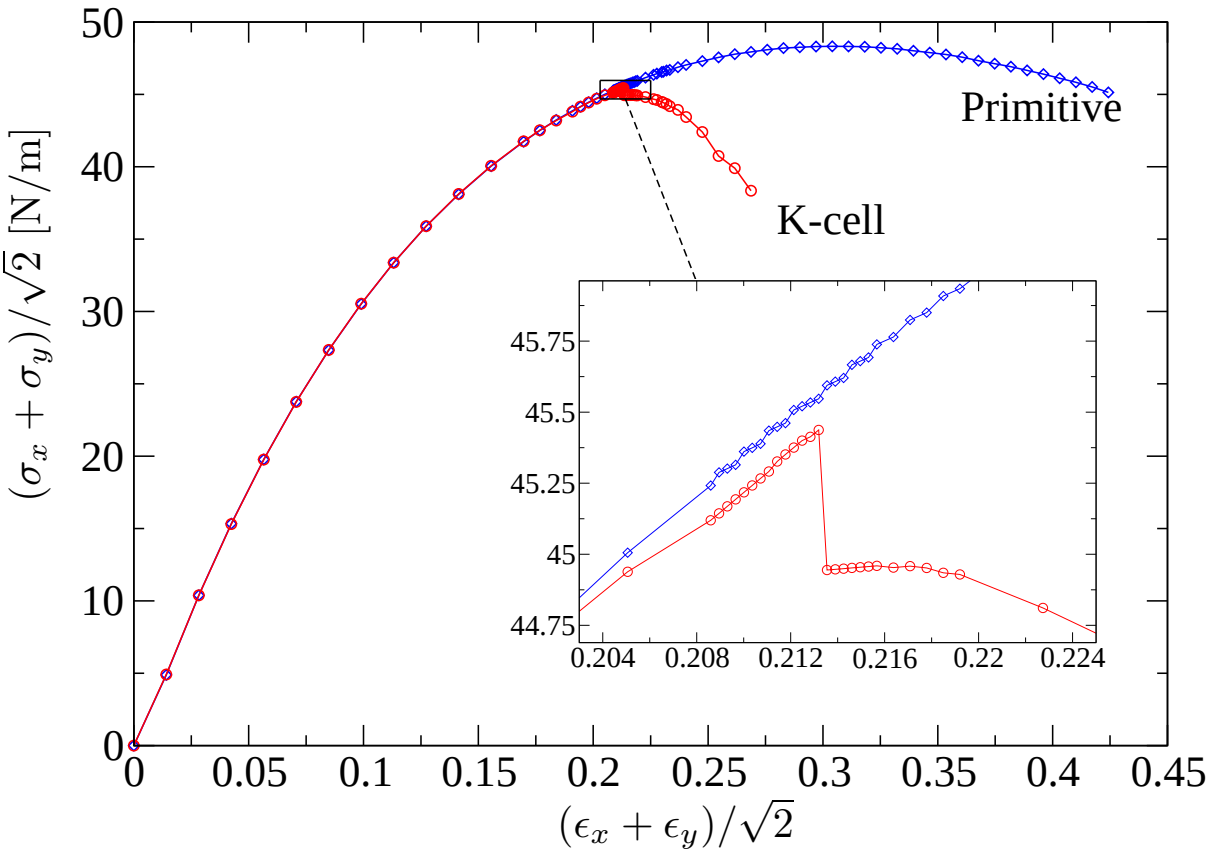
Primitive
K-cell
$(\sigma_x + \sigma_y)/\sqrt{2}$ [N/m]
$(\epsilon_x + \epsilon_y)/\sqrt{2}$
0
10
20
30
40
50
0
0.05
0.1
0.15
0.2
0.25
0.3
0.35
0.4
0.45
44.75
45
45.25
45.5
45.75
0.204
0.208
0.212
0.216
0.22
0.224

Figure 3:

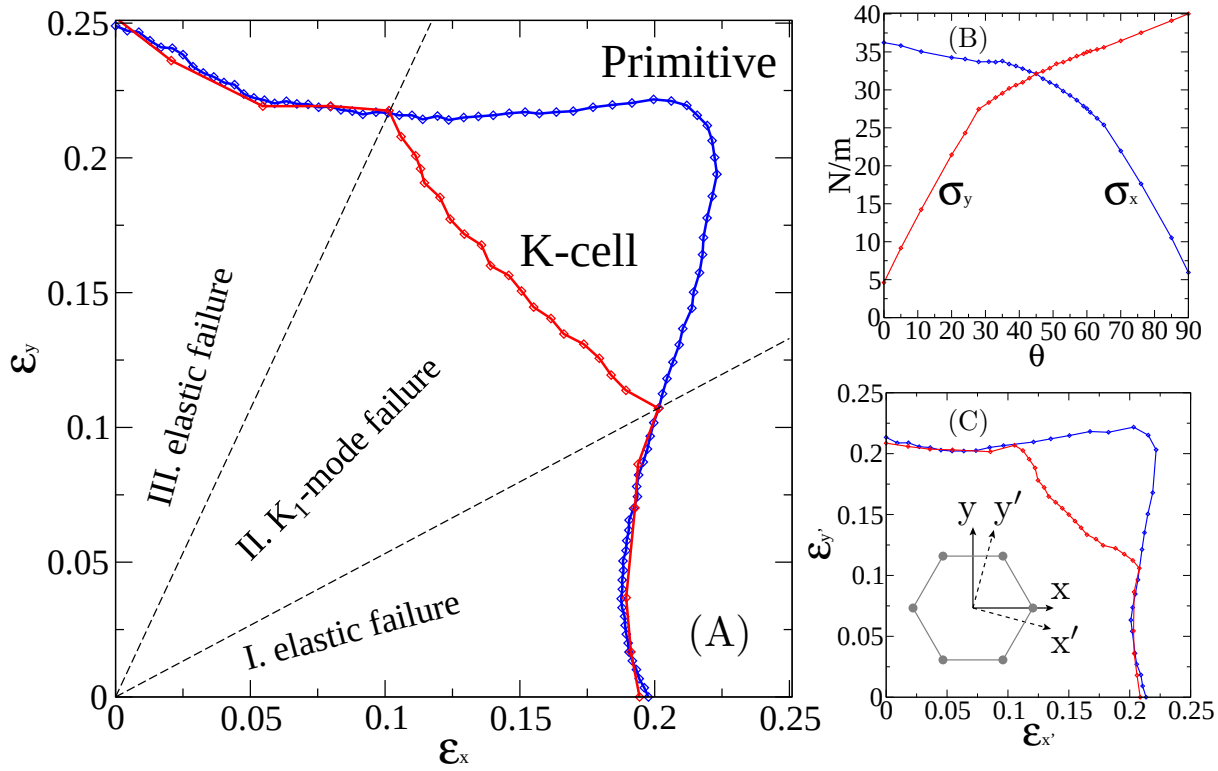
Primitive
K-cell
III. elastic failure
II. K1-mode failure
I. elastic failure
(A)
(B)
(C)
N/m
θ
σy
σx
εy
εx
εy'
εx'
y
y′
x
x′

Figure 4: